Article

Properties of Scattering Fields from Gaussian Beam Incident on Rough Cylinders

Shubing Ye [1], Guobin Feng [2], Zhejun Feng [1], Zhenbao Wang [2], Dahui Wang [2] and Changqing Cao [1,*]

1   School of Optoelectronic Engineering, Xidian University, Xi'an 710071, China; sbye@stu.xidian.edu.cn (S.Y.)
2   State Key Laboratory of Laser Interaction with Matter, Northwest Insitute of Nuclear Technology, Xi'an 710024, China
*   Correspondence: chqcao@mail.xidian.edu.cn

Abstract: At present, most researchers focus on plane wave incident on targets, but in practical applications, most of the beams are Gaussian beam. We study the scattering fields of Gaussian beam incident on rough cylinders. Coherent and incoherent scattering coefficients are obtained based on the angular spectrum expansion and physical optics approximation, and the effects of cylinder roughness, beam radius, cylinder radius and angle of incidence on scattering coefficients are analyzed. The results show that, for a constant wavelength, when the root mean square height is greater than or equal to 1/5 of the wavelength, the coherent scattering coefficient curve undergoes a change in its distribution, with the peak transforming into a trough. Furthermore, when the root mean square height is greater than or equal to 1/3 of the wavelength, the incoherent scattering coefficient experiences a decline as the root mean square height increases. The correlation length only affects the incoherent scattering coefficient. Both the coherent and incoherent scattering coefficients decrease with the increase in the incident angle. Finally, when the roughness and incident angle are constant, with the increase in the ratio of the cylinder radius to the beam waist radius, the scattered light field is more concentrated. Our results provide the theoretical basis for the measurement of the cylindrical scattering field.

Keywords: rough cylinder; Gaussian beam; scattering field

1. Introduction

In general, the wavelength range of the laser band is from submicron to micron, so the target surface is usually considered rough. The scattered echo usually contains physical information about the target, such as the geometry and electromagnetic properties [1]. In the fields of civil and commercial pursuits, research on the scattering echo properties of crops can monitor their growth environment and condition, and concurrently mitigate the economic repercussions resulting from natural calamities [2]. By means of studying the scattered echo information of land and oceanic surfaces, crucial information pertaining to ground height variation, soil moisture levels, seawater dielectric constant, temperature, salinity, wave height and wave cycle can be obtained; such findings may prove advantageous in terms of environmental monitoring and natural disaster predictions [3]. Thus, the research of the scattering field of random rough surfaces holds immense value and significance. To conduct a thorough exploration of the scattering field of three-dimensional rough targets, it is imperative to frequently adjust the incident angles of the light source and receiving positions, while also generating diverse random rough targets. Despite the feasibility of directly measuring the scattering field, comprehending the impact of the incident beam angle, surface roughness, and various other factors on the scattered field often proves challenging. Furthermore, establishing the physical model of light scattering applicable to three-dimensional random rough targets for experimental evaluation remains a formidable task [4,5]. As a result, researchers both domestically and internationally

have continually proposed numerous computational techniques aimed at investigating the scattering properties of rough surfaces via simulation. In this paper, the physical optics method is used to study the scattering characteristics. This method yields precise calculation outcomes for large-scale targets, while also boasting a swift calculation speed and straightforward physical procedures [6,7].

Berlasso studied the autocorrelation function of the scattering field by plane waves incident on a rough cylindrical surface and analyzed through simulations the relation between the autocorrelation function and the roughness/angle [8]. The team of researchers considered rough spheres, cones and cylinders to study the statistical properties of scattered fields after plane wave incidence and deduced the coherent and incoherent scattering cross-sections, mutual coherence functions, and fourth-order moments of the scattered field. These researchers mainly discussed and analyzed the effects of surface roughness, three-dimensional dimensions and incident angles on the statistical properties. Different types of light sources have different scattering fields incident on the same target, and in practice, Gaussian beams are often laser light sources [9,10]. Collin first studied the scattering characteristics of Gaussian beam and rough surface two-dimensional conductors, mainly for two-dimensional flat objects [11]. H. Chen et al. considered spheres to study the statistical properties of the scattering fields of Gaussian beam incident on rough three-dimensional targets and analyze the effects of surface roughness, sphere radius and incident beam waist radius on the scattering cross-section. In addition, they compared incoherent scattering cross-sections with the results of plane wave incidence [12]. Gerald M. first converted the Gaussian beam into a plane wave, and then studied the scattering problem of the Gaussian beam incident on the rough metal surface [13]. There have been many research works on the propagation characteristics and the effects of initial perturbation of Gaussian wave packets during propagation [14–19].

The research on the scattering fields of rough cylinders has primarily focused on the plane wave, with a dearth of research concerning the statistical properties of the scattering field when subjected to Gaussian beam incidence. Furthermore, it should be noted that the results from the scattering phenomena of rough planes, spheres and cones under various types of incident beams cannot be readily applied to rough cylinders [20,21]. Moreover, a large number of targets in light detection and ranging, remote sensing, and target identification exhibit cylindrical shapes. As a result, comprehensive research of the scattering fields resulting from the incidence of Gaussian beam on rough cylinders may serve as a crucial foundation for, and offer technical assistance to, practical applications.

In this study, we used the methods of angular spectrum expansion and physical optics approximation to study the characteristics of the scattering field resulting from the incidence of Gaussian beam on rough cylinders. Our analysis, employing the physical optics approximation method, enabled us to deduce the distribution of the scattering field. The scattering field resulting from scattering from rough surfaces can be partitioned into two distinct components: coherent and incoherent scattered fields. The formulas for the scattering coefficients associated with these two components were derived. In order to gain insights into the variations of the coherent and incoherent scattering coefficients, numerical simulations have been conducted based on different types of roughness, incident angles, waist radius and cylinder radius.

2. Scattering Field of Rough Cylinder

We built the scattering model as shown in Figure 1a; defined the target coordinate system to be OXYZ and the incident field coordinate system to be $O_iX_iY_iZ_i$. The OXYZ coordinate system was located at the center of the cylinder, and the Y-axis was parallel to the axis of the cylinder. The Gaussian beam along axis Z_i propagated, and $Z_i = 0$ was the beam waist plane of the incident Gaussian beam. The incident angles and incident azimuth were θ_i and φ_i, the scattering angles and azimuth angles were θ_s and φ_s, l_0 was the incident distance, which signifies the distance from the incident position O_i to the origin of the target coordinate system O. Figure 1b depicts a lateral view of the cylindrical structure receiving

Gaussian beam illumination. The cylinder with radius a and infinite length, and its surface roughness conformed to the Gaussian probability distribution, as shown in Figure 2.

(a)   (b)
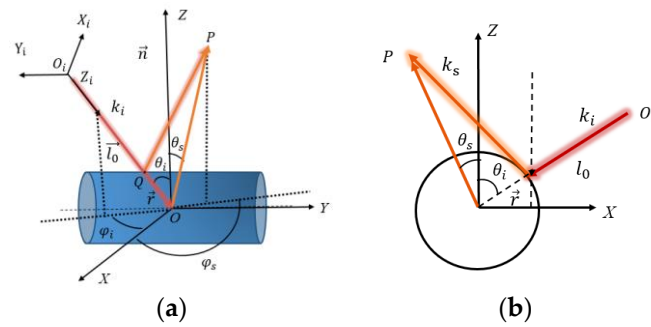
Figure 1. Gaussian beam incident on the rough cylinder. (**a**) Schematic diagram of beam incident cylinder; (**b**) schematic diagram of the side of a rough cylinder with Gaussian beam incident. θ_i and φ_i represent the incident angles and incident azimuth, θ_s and φ_s represent the scattering angles and azimuth angles.
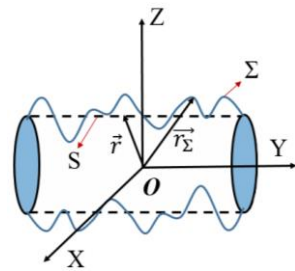
Figure 2. Sketch map of rough cylindrical surface details. $\vec{r}_\Sigma$ and $\vec{r}$ are the distances from the center of the target coordinate system to rough surface Σ and smooth cylinder S.

Figure 2 shows details of the rough cylinder, which was composed of a smooth cylinder with added random roughness features by $\xi(\vec{r})$, where $\xi(\vec{r})$ indicates that any point on the rough surface satisfies the Gaussian distribution and where $\vec{r}_\Sigma$ and $\vec{r}$ are the distances from the center of the target coordinate system to the rough surface Σ and smooth cylinder S, respectively; $\vec{r}_\Sigma = \vec{r} + \vec{n}\xi(\vec{r})$, where $\vec{n}\xi(\vec{r})$ represents the random roughness distribution on the cylindrical surface and the $\vec{n}$ represents the normal vector of the incident point.

Disregarding the temporal characteristics $\exp(i\omega t)$, the incident Gaussian beam is [12]:

$$E_i(x_i, y_i, 0) = \exp\left(-\frac{x_i^2 + y_i^2}{\omega_0^2}\right) \tag{1}$$

By means of the angular spectrum expansion method and transformation of coordinate axes [22], the Gaussian beam can be expressed as a composite of numerous plane waves [12]:

$$E_i\left(\vec{r}\right) = \frac{1}{4\pi^2 \cos\theta_i} \iint f(k_x, k_y) \exp\left(-i\vec{k} \cdot \left(\vec{r}_\Sigma - \vec{l}_0\right)\right) dk_x dk_y \tag{2}$$

$$f(k_x, k_y) = \omega_0^2 \pi \exp\left[-\frac{g(k_x, k_y)}{4}\omega_0^2\right] \tag{3}$$

$$g(k_x, k_y) = \left(k_x \cos\theta_i \cos\varphi_i + k_y \cos\theta_i \sin\varphi_i + k_z \sin\theta_i\right)^2 + \left(k_x \sin\varphi_i - k_y \cos\varphi_i\right)^2 \tag{4}$$

Based on the Kirchhoff approximation, it is feasible to derive the scattered light field expression resulting from the interaction of a rough cylinder with incident plane wave [23]:

$$E_s(\vec{r}) = \frac{i}{4\pi} \int \vec{k}_{i\_s} \cdot \vec{n} R(\theta_i) \exp\left[i\vec{k}_{i\_s} \cdot \vec{n}\zeta\left(\vec{r}\right)\right] \frac{\exp\left\{-ik\left[\rho(\vec{d},\vec{r}) + \phi(\vec{r})\right]\right\}}{\rho(\vec{d},\vec{r})} ds' \quad (5)$$

Each term in the formula presented: $\vec{k}_{i\_s} = \vec{k}_i - \vec{k}_s$, indicates the vector difference between the incident beam and the scattered beam; $R(\theta_i)$ indicates the Fresnel reflection coefficient at the surface rough object $\vec{r}$, θ_i is the incidence angle; $\exp[i\vec{k}_{i\_s} \cdot \vec{n}\zeta\left(\vec{r}\right)]$ represents the additional phase factor introduced by the random undulations of the surface of the rough object; $\exp\left\{-ik[\rho(\vec{d},\vec{r}) + \phi(\vec{r})]\right\}$ represents the transmission distance causing a phase change, where $\rho(\vec{d},\vec{r}) = \left|\vec{d} - \vec{r}\right|$, $\phi(\vec{r}) = \vec{k}_i \cdot \vec{r}$.

Based on the theory of rough surface scattering, the scattering field associated with a Gaussian beam can be articulated as the linear sum of the scattering fields of various plane waves. By integrating Formulas (2) and (5), the scattering field distribution of the Gaussian beam incident can be obtained as:

$$E_s(\vec{r}) = \frac{i}{16\pi^3 \cos\theta_0} \iint dk_x dk_y \int \vec{k}_{i\_s} \cdot \vec{n} R(\theta_i) \exp\left[-i\vec{k}_{i\_s} \cdot \vec{n}\zeta(\vec{r})\right]$$
$$\times f(k_x, k_y) \exp\left[-i\vec{k} \cdot (\vec{r}_\Sigma - \vec{l}_0)\right] \frac{\exp\left\{-ik\left[\rho(\vec{d},\vec{r}) + \phi(\vec{r})\right]\right\}}{\rho(\vec{d},\vec{r})} ds' \quad (6)$$

The above formula θ_0 represents the mirror reflection angle. Given that the distance $\vec{r}_i = \vec{r}_\Sigma - \vec{l}_0$ from the waist radius of the incident beam to the surface of the rough object exceeds the incident wavelength significantly, the exponential factor $\exp[-i\vec{k} \cdot (\vec{r}_\Sigma - \vec{l}_0)]$ exhibits rapid oscillations in k-space; solely the integral value proximal to the stable phase point confers any significance and contribution [12]. Hence, the subsequent phase uses the stable phase method to solve the integral regarding k_x and k_y as prescribed in Formula (6), and takes advantage of the zero-point approximation and the first-order approximation, and finally simplifies it to:

$$E_s(\vec{r}) = \frac{i\omega_0^2 \exp(-ikl_0)}{16\pi^2 \cos\theta_0} \int \exp\left[-\frac{k^2\omega_0^2 g_0(\vec{r}_\Sigma)}{4l_0^2}\right] \vec{k}_{i\_s} \cdot \vec{n} R(\theta_i)$$
$$\times \frac{\exp\left\{-ik\left[\rho(\vec{d},\vec{r}) + \phi(\vec{r})\right]\right\}}{\rho(\vec{d},\vec{r})} \exp[-i\vec{k}_{i\_s} \cdot \vec{n}\zeta(\vec{r})] ds' \quad (7)$$

$$g_0\left(\vec{r}_\Sigma\right) = (x_\Sigma \cos\theta_i \cos\varphi_i + y_\Sigma \cos\theta_i \sin\varphi_i + z_\Sigma \sin\theta_i)^2 + (x_\Sigma \sin\varphi_i - y_\Sigma \cos\varphi_i)^2$$

When the dimensions of an object far exceed the roughness of the surface, the amplitude term in the relevant formula x_Σ, y_Σ, z_Σ may be replaced by the coordinates x, y, and z, where x_Σ, y_Σ and z_Σ, respectively, represent the distance from any point on the rough cylindrical surface to the coordinate axis in the target coordinate system, and Formula (7) can be simplified:

$$E_s(\vec{r}) = \frac{i\omega_0^2 \exp(-ikl_0)}{16\pi^2 \cos\theta_0} \int \exp\left[-\frac{k^2\omega_0^2 g_0(\vec{r})}{4l_0^2}\right] \vec{k}_{i\_s} \cdot \vec{n} R(\theta_i)$$
$$\times \frac{\exp\left\{-ik\left[\rho(\vec{d},\vec{r}) + \phi(\vec{r})\right]\right\}}{\rho(\vec{d},\vec{r})} \exp\left[-i\vec{k}_{i\_s} \cdot \vec{n}\zeta(\vec{r})\right] ds' \quad (8)$$

To clarify the influence of various factors on the scattering field, we performed and analyzed the formulations and numerical calculations of coherent and incoherent scattering coefficients.

3. Numerical Analysis of Coherent Scattering Coefficient

According to the scattering field theory of rough surfaces [12], the distribution of coherent scattering field represents the ensemble average of the light field on the receiving position. The coherent scattering field of Gaussian beam incidence on the rough cylindrical surfaces is given by:

$$
\begin{aligned}
< E_s^c(\vec{r}) > = \frac{i\omega_0^2 \exp(-ikl_0)}{16\pi^2 \cos\theta_0} \int \exp\left[-\frac{k^2\omega_0^2 g_0(\vec{r})}{4l_0^2}\right] \vec{k}_{i\_s} \cdot \vec{n} R(\theta_i) \\
\times \frac{\exp\left\{-ik\left[\rho(\vec{d},\vec{r})+\phi(\vec{r})\right]\right\}}{\rho(\vec{d},\vec{r})} \chi(\vec{k}_{i\_s} \cdot \vec{n}) ds'
\end{aligned}
\tag{9}
$$

where $\chi(\vec{k}_{i\_s} \cdot \vec{n}) = \left\langle \exp\left[-i\vec{k}_{i\_s} \cdot \vec{n}\zeta(\vec{r})\right]\right\rangle$ represents the impact of height fluctuations on the root mean square [12], $<\dots>$ this operator represents averaging the function. By comparing Equation (9) with the coherent scattering field of plane wave incident on a smooth cylindrical surface [23], the field of Gaussian beam incident on a rough cylindrical surface can be expressed as:

$$
< E_s^c(\vec{r}) > = \frac{ik\omega_0^2}{16\pi^2 \cos\theta_0} \exp\left[-\frac{k^2\omega_0^2 g_0(\vec{r})}{4l_0^2}\right] \vec{k}_{i\_s} \cdot \vec{n} R(\theta_i)\chi(\vec{k}_{i\_s} \cdot \vec{n}) E_s^p(\vec{r})
\tag{10}
$$

where $E_s^p(\vec{r})$ denotes the scattering field of plane wave incident on the rough cylinder, according to the definition of scattering coefficient [24], we have

$$
\sigma_c = \frac{4\pi l_0^2 \left|< E_s^c(\vec{r}) >\right|^2}{I_i} = \frac{|R(\theta_i)|^2 \chi^2\left(\vec{k}_{i\_s} \cdot \vec{n}\right)\sigma_g}{f}
\tag{11}
$$

where $\sigma_g = \pi a \cos\left(\frac{\theta_s}{2}\right)$ is the coherent scattering coefficient of plane wave incident on the smooth cylindrical surface [25], $\chi^2\left(\vec{k}_{i\_s} \cdot \vec{n}\right) = \exp\left[-\left(\vec{k}_{i\_s} \cdot \vec{n}\right)^2 \delta^2/2\right]$. The function f representing Gaussian beam factor is given by

$$
\begin{aligned}
f &= \int \exp\left\{-\frac{k^2\omega_0^2\left[g(\vec{r})-g_0(\vec{r}_0)\right]}{2l_0^2}\right\} ds / \int ds \\
&= \int \exp\left\{-2\alpha^2\left[h(\vec{r})-h_0(\vec{r}_0)\right]\right\} ds / \int ds
\end{aligned}
\tag{12}
$$

$$
\begin{aligned}
h(\vec{r}) &= (\tan\theta\cos\varphi\cos\theta\cos\varphi + \tan\theta\sin\varphi\cos\theta\sin\varphi + z_\Sigma'\sin\theta/a)^2 \\
&\quad + (\tan\theta\cos\varphi\sin\varphi - \tan\theta\sin\varphi\cos\varphi)^2
\end{aligned}
\tag{13}
$$

where $\alpha = a/\omega$ is the ratio of the cylinder radius to the incident beam radius, $\omega = 2l_0/(k\omega_0)$, $\int ds$ represents the integral of the area irradiated by the Gaussian beam. Through numerical calculation, we analyzed the influence of different factors on σ_c. In the context of cylinder surfaces, the surface roughness is about the wavelength of the incident radiation, with different wavelengths yielding different degrees of roughness on the same surface. The quantitative assessment of cylinder surface roughness is dependent on two key factors, namely, the root mean square height (δ) and the correlation length (cl) of the surface. Formula (11)

suggests that the distribution of the coherent scattered light field remains unaltered by the correlation length. Thus, in order to investigate the impact of δ on the coherent scattering coefficient, simulations were carried out under specific wavelength conditions of 0.532, 1.064 and 1.550 µm. The material of the rough cylinder was assigned as aluminum [26], and the corresponding refractive index parameter $n = 0.94 + 6.41i$, $2.43 + 10.7i$ and $1.58 + 15.66i$, the incident angle $\theta_i = 30°$, the incident azimuth $\varphi_i = 0°$, and the receiving azimuth $\varphi_s = \varphi_i + \pi$.

According to Figure 3a, it can be inferred that the coherent scattering coefficient gradual decreases as the δ increases, eventually reaching its maximum level at the specular scattering angle. Notably, a shift in the shape of the coherent scattering coefficient distribution curve was observed when the $\delta \geq 0.1$ µm. Figure 3b demonstrates that the minimum value of the coherent scattering coefficient occurred at the specular scattering angle, and that it exhibited a continuous decrease with a rise in the δ. In Figure 3c,d, when the wavelength was 1.064 µm, it was observed that the spatial distribution of the coherent scattering coefficient underwent a change when the $\delta \geq 0.2$ µm. In Figure 3e,f, at a wavelength of 1.550 µm, it was observed that the spatial distribution of the coherent scattering coefficient underwent a change when the $\delta \geq 0.3$ µm. In summary, it can be inferred that under constant incident wavelength conditions, the coherent scattering coefficient experiences a gradual decrease with a rise in the δ, and when $\delta \geq 1/5\ \lambda$, the spatial curve of the coherent scattering coefficient changes from a peak to a trough.
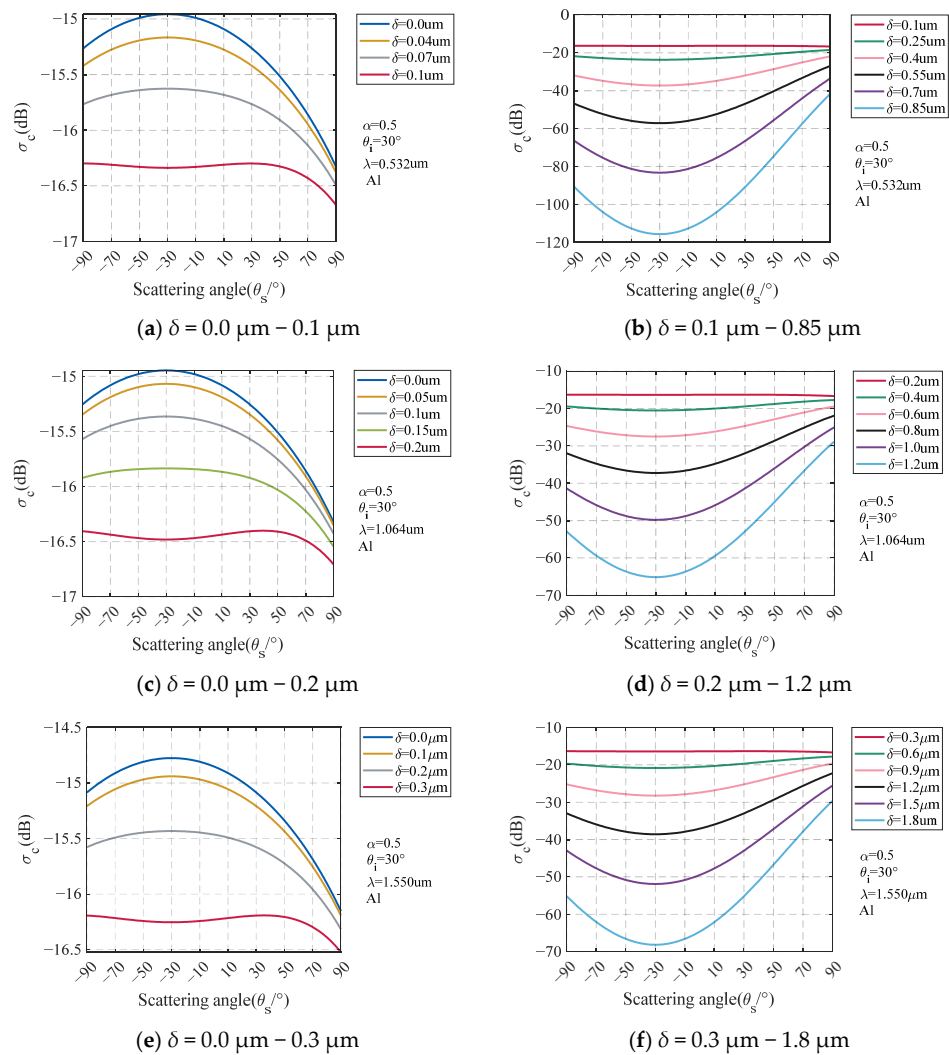
Figure 3. The effects of different wavelengths and root mean square height on coherent scattering coefficient.

Figure 4 shows the effect of α on the coherent scattering coefficient under different incident angles. In the case of a relatively smooth cylindrical surface $\delta = 0.1$ µm, with the increase in α, the coherent scattering coefficient increased gradually; however, when $\alpha \geq 4$, the coherent scattering coefficient displayed an upward trend near the specular scattering angle, with a corresponding decline observed in the case of other scattering angles. The phenomenon can be attributed to the reduction in beam waist radius of the incident beam, resulting in a reduction in the contact range between the incident beam and the cylindrical surface, the energy of the scattered field becoming more concentrated. When considering various incident angles, an increase in the incident angle does not significantly alter the distribution of the coherent scattering coefficient curve. Rather, it only affects the change in the scattering coefficient amplitude. Notably, when the incident angle is at 90°, the change in α has almost the same effect on the coherent scattering coefficient. The coherent scattering coefficient exhibits a variation with respect to the incident angle, and its maximum value position also undergoes a shift.
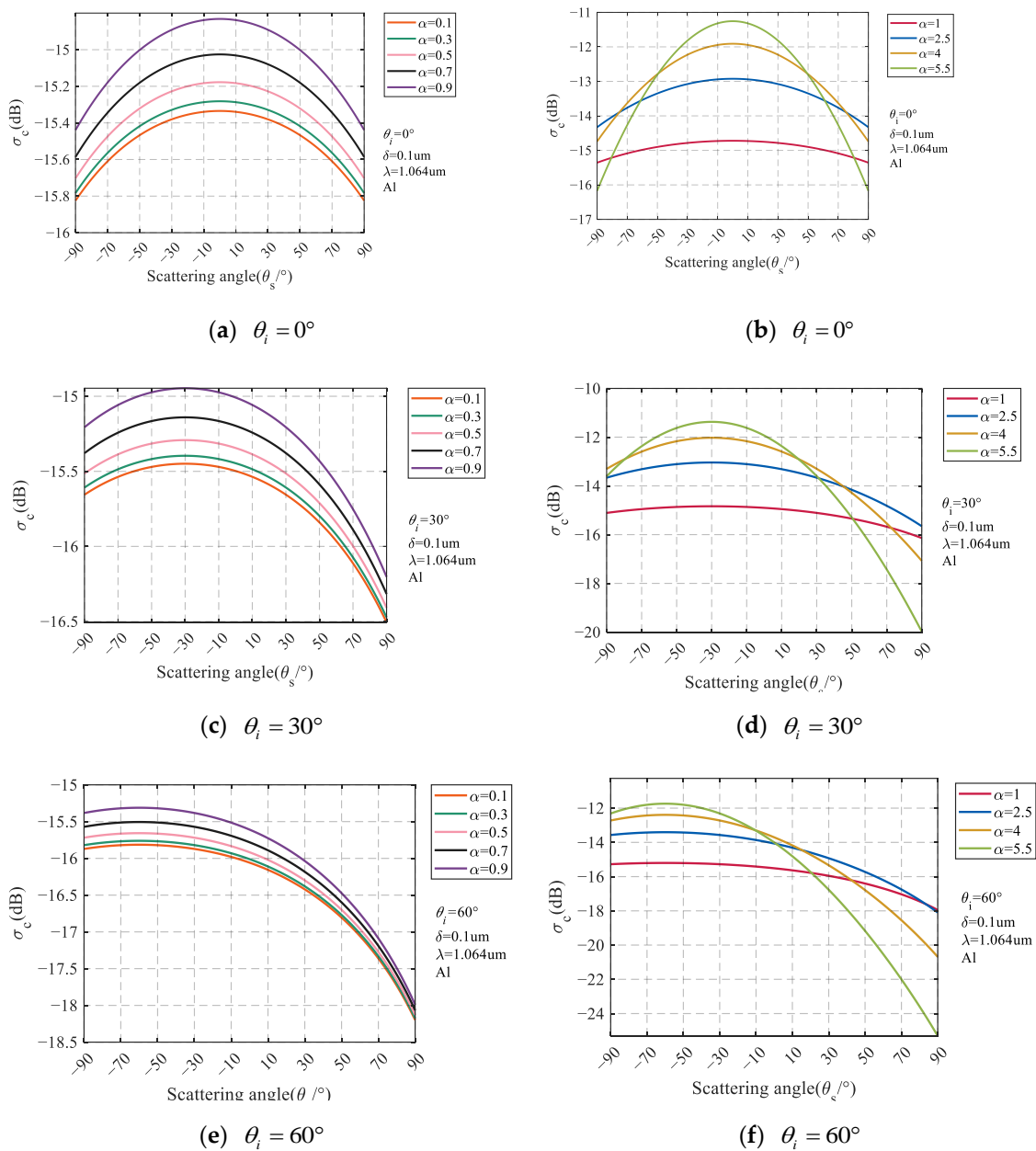
(**a**) $\theta_i = 0°$ (**b**) $\theta_i = 0°$

(**c**) $\theta_i = 30°$ (**d**) $\theta_i = 30°$

(**e**) $\theta_i = 60°$ (**f**) $\theta_i = 60°$

Figure 4. *Cont.*

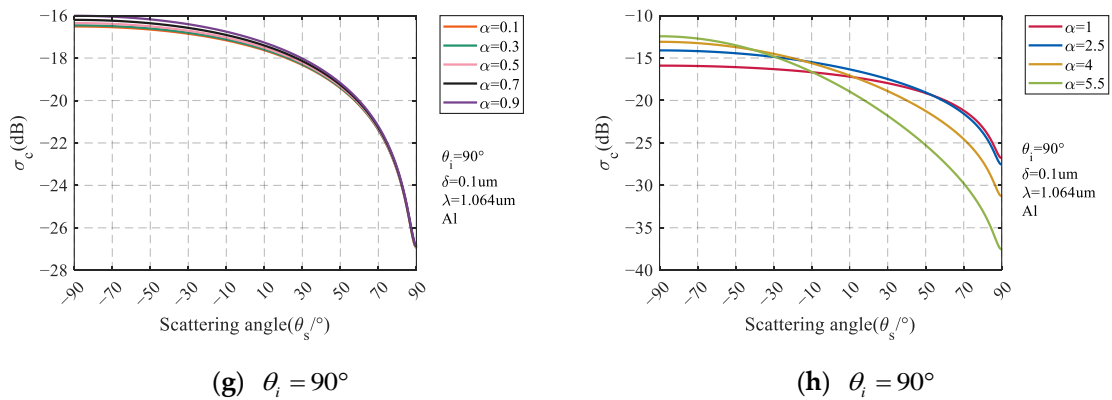(**g**) $\theta_i = 90°$

(**h**) $\theta_i = 90°$

Figure 4. The effect of α on the coherent scattering coefficient under different incident angles.

4. Numerical Analysis of Incoherent Scattering Coefficient

A rough target surface will cause diffuse reflection; we derived and simulated the incoherent scattering cross-section of the scattering field:

$$\left\langle \left| E_s\left(\vec{r}\right) \right|^2 \right\rangle = \left\langle E_s\left(\vec{r}\right) E_s^*\left(\vec{r}\right) \right\rangle - \left| \left\langle E_s\left(\vec{r}\right) \right\rangle \right|^2 \tag{14}$$

Combined with the field distribution in Equation (9), the mutual coherence function can be obtained as:

$$
\begin{aligned}
\left\langle E_s^c\left(\vec{r}\right) E_s^{c*}\left(\vec{r}\right) \right\rangle = {}& \left(\frac{1}{16\pi^2 \cos\theta_0}\right)^2 \int ds' \int ds'' \, \vec{k}_{i\_s} \cdot \vec{n} \, R(\theta_i) \vec{k}_{i\_s} \cdot \vec{n}' R(\theta_i') \\
& \times \exp\left[-\frac{k^2\omega_0^2}{2l_0^2}\left(g_0\left(\vec{r}\right) + g_0\left(\vec{r}'\right)\right)\right] \\
& \times \left\langle \exp\left[i\vec{k}_{i\_s} \cdot \vec{n}\,\zeta\left(\vec{r}\right) - i\vec{k}_{i\_s} \cdot \vec{n}'\zeta\left(\vec{r}'\right)\right]\right\rangle \\
& \times \frac{\exp\left\{ik\left[\rho\left(\vec{d},\vec{r}\right)+\phi\left(\vec{r}\right)\right]-ik\left[\rho\left(\vec{d},\vec{r}'\right)+\phi\left(\vec{r}'\right)\right]\right\}}{\rho\left(\vec{d},\vec{r}\right)}
\end{aligned}
\tag{15}
$$

Then, using Equations (9) and (15) in Equation (14), the incoherent scattering field can be obtained as:

$$
\begin{aligned}
\left\langle \left| E_s\left(\vec{r}\right) \right|^2 \right\rangle = {}& \left(\frac{k\omega_0^2}{16\pi^2 \cos\theta_0}\right)^2 \int ds' \int ds'' \, \vec{k}_{i\_s} \cdot \vec{n} \, R(\theta_i) \vec{k}_{i\_s} \cdot \vec{n}' R(\theta_i') \\
& \times \exp\left[-\frac{k^2\omega_0^2}{2l_0^2}\left(g_0\left(\vec{r}\right) + g_0\left(\vec{r}'\right)\right)\right] \\
& \times \frac{\exp\left\{ik\left[\rho(\vec{d},\vec{r})+\phi\left(\vec{r}\right)\right]-ik\left[\rho(\vec{d},\vec{r}')+\phi\left(\vec{r}'\right)\right]\right\}}{\rho(\vec{d},\vec{r})} \\
& \times \left[\chi_t\left(\vec{k}_{i\_s} \cdot \vec{n}, \vec{R}_{\Sigma_\perp}\right) - \chi^2\left(\vec{k}_{i\_s} \cdot \vec{n}\right)\right]
\end{aligned}
\tag{16}
$$

To simplify Equation (16), we assumed that the radius of the cylinder was much larger than the incident wavelength and *cl*, and the *R* was much larger than the target, $k_{i\_s} \cdot n' \approx k_{i_s} \cdot n''$, $R(\theta_i') \approx R(\theta_i'')$. Moreover, using tangent planes to approximate integral

ds'' as $dR_{\Sigma_\perp}$ and combining with the far-field approximation, where $dR_{\Sigma_\perp}$ represents the tangent plane of the point, the simplified Equation (16) is given by:

$$
\left\langle \left| E_s\left(\vec{r} \right) \right|^2 \right\rangle = \left(\frac{k\omega_0^2}{4\pi^2 l_0 R} \right)^2 \int ds' \int dR_{\Sigma_\perp} \left(\vec{k}_{i\_s} \cdot \vec{n} R(\theta_i) \right)^2
$$
$$
\times \exp\left[-\frac{k^2\omega_0^2}{2l_0^2} \left(g_0\left(\vec{r} \right) + g_0\left(\vec{r}' \right) \right) \right]
$$
$$
\times \frac{\exp\left\{ ik\left[\rho(\vec{d},\vec{r}) + \phi(\vec{r}) \right] - ik\left[\rho(\vec{d},\vec{r}') + \phi(\vec{r}') \right] \right\}}{\rho(\vec{d},\vec{r})}
$$
$$
\times \left[\chi_t\left(\vec{k}_{i\_s} \cdot \vec{n}, \vec{R}_{\Sigma_\perp} \right) - \chi^2\left(\vec{k}_{i\_s} \cdot \vec{n} \right) \right]
\tag{17}
$$

where the functions describing the rough surface are given by $\chi^2\left(\vec{k}_{i\_s} \cdot \vec{n} \right) = \exp\left[-\left(\vec{k}_{i\_s} \cdot \vec{n} \right)^2 \delta^2/2 \right]$ and $\chi_t\left(\vec{k}_{i\_s} \cdot \vec{n}, \vec{R}_{\Sigma_\perp} \right) = \exp\left[-\left(\vec{k}_{i\_s} \cdot \vec{n} \right)^2 \delta^2(1 - \langle \xi_1\xi_2 \rangle) \right]$, representing the two-dimensional characteristic function of the rough cylinder, with $\langle \xi_1\xi_2 \rangle = \delta^2 \exp\left(-\frac{R_s^2}{cl^2} \right)$ representing the rough surface correlation, R_s represents the distance between two adjacent points on a rough surface. By comparing Equation (17) with the formulation in Ref. [9], the second integral in Equation (17) represents the incoherently scattered field distribution of the plane wave incident on the rough cylinder. According to the definition of scattering coefficient, the incoherent scattering coefficient σ_i is:

$$
\sigma_i = \frac{4\pi l_0^2 \left\langle \left| E_s\left(\vec{r} \right) \right|^2 \right\rangle}{I_i}
$$
$$
= \frac{\left\{ \frac{k\omega_0^2}{4\pi^2 l_0 d} \left[\vec{k}_{i\_s} \cdot \vec{n} R(\theta_i) \right] \right\}^2 \int \exp\left[-\frac{k^2\omega_0^2}{2l_0^2} g_0\left(\vec{r} \right) \right] \sigma_p ds'}{I_i}
\tag{18}
$$

Simplifying the above formula:

$$
\sigma_i = \frac{A^2 \int \exp\left[-2\alpha^2 h_0(\theta, \varphi, z'_\Sigma) \right] \sigma_p ds'}{I_i}
\tag{19}
$$

$$
h_0(\theta, \varphi, z_\Sigma') = (\tan\theta \cos\varphi \cos\theta_0 \cos\varphi_0 + \tan\theta \sin\varphi \cos\theta_0 \sin\varphi_0 + z_\Sigma' \sin\theta_0/a)^2
$$
$$
+ (\tan\theta \cos\varphi \sin\varphi_0 - \tan\theta \sin\varphi \cos\varphi_0)^2
\tag{20}
$$

In Equation (19), σ_p is the incoherent scattering of plane waves incident on the rough cylinder obtained from Ref. [9]. Therefore, using this formulation, we performed numerical calculation analysis concerning the cylinder roughness, incident angle, cylindrical radius and waist radius.

Figure 5 shows the relationship between δ and σ_i under different λ. In Figure 5a, with the increase in δ, the incoherent scattering coefficient increased accordingly, and the maximum value of the incoherent scattering coefficient was near the mirror scattering angle, but when $\delta = 0.17$ μm, the σ_i of the mirror scattering angle decreased. In Figure 5b, the incoherent scattering coefficient decreased with the increase in δ, and reached the minimum value near 0°. It can be seen from Figure 5c,d that when the incident wavelength was 1.064 μm, the spatial distribution of the incoherent scattering coefficient changed when $\delta \geq 0.36$ μm. In Figure 5e,f, when the wavelength was 1.550 μm, the incoherent scattering coefficient curve changed when $\delta \geq 0.5$ μm. In summary, at a constant wavelength, the incoherent scattering coefficient gradually decreased with the increase in the δ, and when $\delta \geq 1/3\lambda$, the spatial curve of the incoherent scattering coefficient changed, it approached a minimum value $\theta_s = 0°$. The reason for the change in the incoherent scattering coefficient

curve is that as the δ increases, the surface roughness of the cylinder changes, so the $\delta \geq 1/3\lambda$, the incoherent scattering coefficient changes.
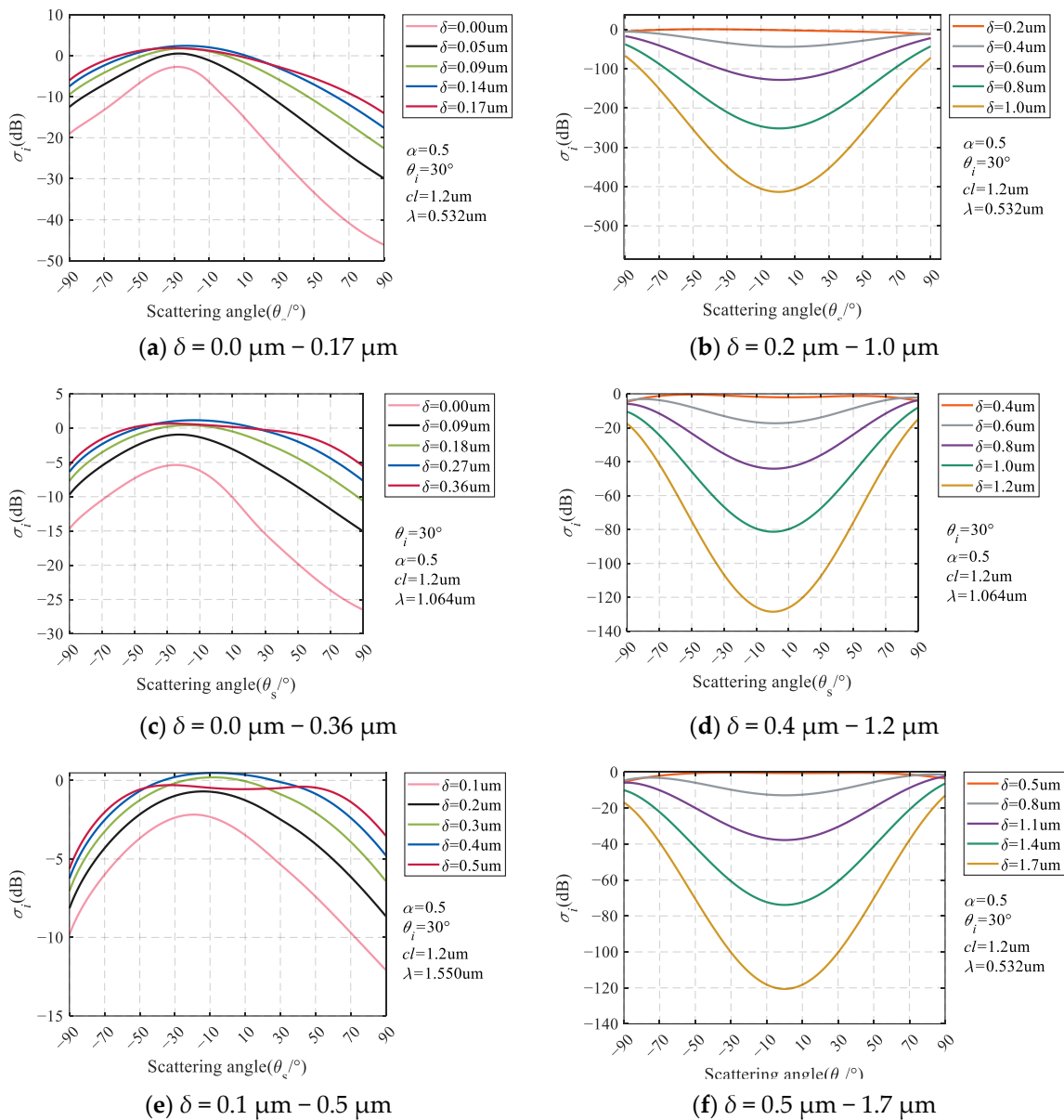
Figure 5. The effects of different wavelengths and root mean square height on incoherent scattering coefficient.

In Figure 6, simulating the incoherent scattering coefficient with correlation lengths under different wavelength conditions, it can be seen that when the roughness was constant, the incoherent scattering coefficient increased with the increase in wavelength, but the change trend did not change. When $\delta = 0.1$ μm, the incoherent scattering coefficient increased with the increase in the correlation length at $\theta_s = -20° \sim -40°$; however, the magnitude of this trend was relatively small. Conversely, at other scattering angles, there was a gradual decrease in the incoherent scattering coefficient as the correlation length increased. As the correlation length escalated, the surface of the cylinder exhibited enhanced smoothness, resulting in a heightened concentration of scattered energy at the mirror angle position, and a proportionate decline in scattered light intensity values at other scattering angles.

(**a**) $\lambda = 0.532$ μm

(**b**) $\lambda = 1.064$ μm

(**c**) $\lambda = 1.550$ μm
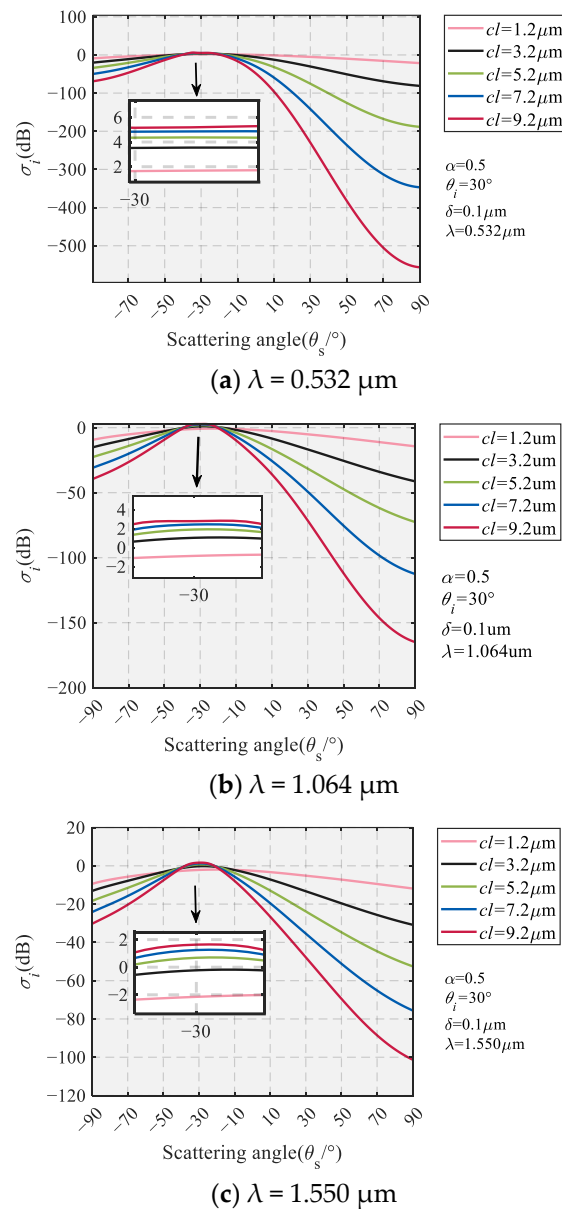
Figure 6. The effects of different correlation lengths on incoherent scattering coefficient.

It can be seen from Figure 7a that when the $\theta_i = 0°$, the light beam was vertically incident on the surface of the cylinder, and the attainment of the maximum value in the vicinity of back scattering. The incoherent scattering coefficient underwent a rapid reduction at the scattering angles situated on either side of the peak, and due to the random distribution of surface roughness, the scattering velocities on both sides of the peak were different. In Figure 7b,c, when the angle of incidence $\theta_i = 10°\sim40°$ was oblique, the maximum scattered light intensity was observed in proximity to the specular scattering point; $\theta_i = 50°$, the maximum value of scattering angle was $-40°$. In Figure 7d, when the $\theta_i \geq 60°$, the maximum scattering angle position was not at the mirror reflection angle position, the maximum of the incoherent scattering coefficient with $\theta_i = 60°$ was at about $\theta_i = -40°$, and the maximum for the $\theta_i = 70°$ was at about $\theta_i = -50°$, and so on. The reason for this phenomenon is that the alteration in incident angle results in a varying contact position between the cylindrical surface and the incident beam.
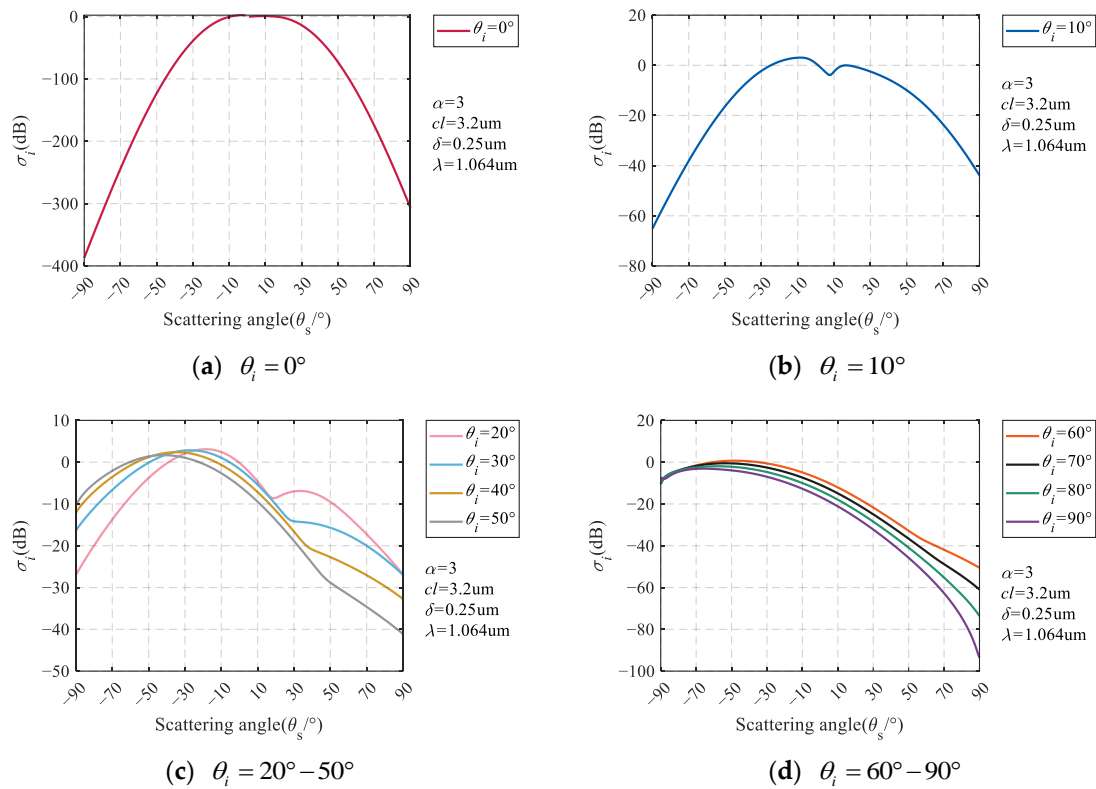
(a) $\theta_i = 0°$

(b) $\theta_i = 10°$

(c) $\theta_i = 20° - 50°$

(d) $\theta_i = 60° - 90°$

Figure 7. The influence of different incident angles on incoherent scattering coefficient.

In normal incidence, the interaction area between the incident beam and the cylindrical surface is moderately even on both sides, resulting in a uniform backscattered light field. For $\theta_i = 10° \sim 50°$, a relatively substantial contact region is established between the incident beam and the cylinder's side, so two locations with larger scattered light intensity can be detected on the receiving plane.

As depicted in Figure 8a, in the scenario of normal incidence, the incoherent scattering coefficient attained its highest value near $\theta_s = 0°$. With the increase in α ($\alpha = a/\omega$), the incoherent scattering coefficient decreases, and the scattered light field becomes more concentrated. In Figure 8b, as the α increased, the mirror scattering angle position was the maximum value, and the $\theta_S = 30°$ was the minimum value. Because of the increase in α, the beam was relatively concentrated, and the surface roughness was small, the scattered beam was mainly concentrated at the mirror scattering angle position. Figure 8c demonstrates that an increase in α corresponds to a more distinct manifestation of two scattering extremes. As shown in Figure 8d, with the increase in α, the incoherent scattering coefficient gradually decreased.
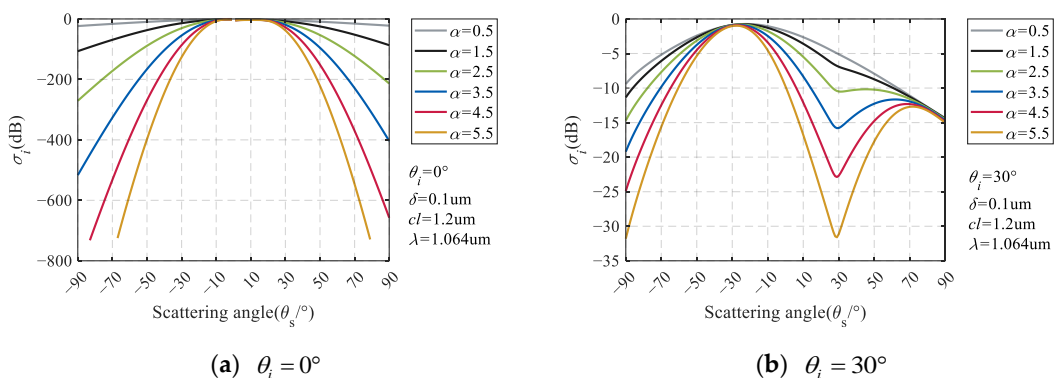

(a) $\theta_i = 0°$

(b) $\theta_i = 30°$

Figure 8. *Cont.*

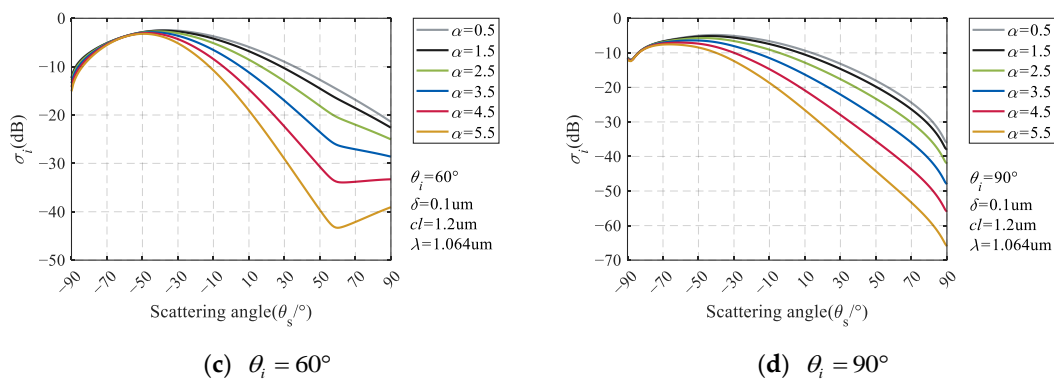**(c)** $\theta_i = 60°$　　　**(d)** $\theta_i = 90°$

Figure 8. The effect of different α on incoherent scattering coefficient.

In summary, with an increasing α, the contact area between the Gaussian beam with decreasing radius and the cylinder surface becomes more and more flat, the scattered field is mainly concentrated near the mirror scattering angle.

5. Discussion

By studying and analyzing the scattering light field, the optical properties of rough surfaces can be better inverted, which can enable more accurate recognition and tracking of rough targets. Using the principles of Kirchhoff approximation and angular spectrum expansion theory, the distribution of the scattering field from a rough cylinder under Gaussian beam illumination was obtained, and the formulas of coherent and incoherent scattering coefficients are presented. Following this, the investigation focused on the impacts of beam parameters, cylinder size, rough surface parameters and incident angle on the coherent and incoherent scattering coefficients. Based on simulation analysis, when the incident wavelengths λ were 0.532, 1.064 and 1.550 μm, and the root mean square height of the surface roughness δ varied from 0 to 1.8 μm, it was found that the coherent scattering coefficient gradually decreased as the δ increased, while the incoherent scattering coefficient initially showed an increasing trend and then a decreasing trend. When the wavelength was fixed, $\delta \geq 1/5\ \lambda$, the distribution of the coherent scattering coefficient curve changed, with the peak becoming a valley; $\delta \geq 1/3\ \lambda$, the incoherent scattering coefficient decreased as δ increased and reached a minimum near 0°. In addition, with the increase in the correlation length, the incoherent scattering coefficient increased near the specular angle while gradually decreasing at other scattering angles. When the roughness and incident angle were constant, as the ratio of cylindrical radius to waist radius increased, the coherent and incoherent scattering widths decreased, resulting in a more concentrated scattering light energy.

6. Conclusions

By using angular spectrum expansion and physical optics approximation to derive the scattering field distribution of the Gaussian beam incident on the rough cylinder, we obtained coherent and incoherent scattering coefficients. Our numerical results indicate that, with a certain wavelength, the coherent scattering coefficient exhibits a gradual decrease with an increase in the root mean square of the height fluctuation. The incoherent scattering coefficient initially increases but then decreases with the same increase in roughness. Moreover, the correlation length only influences the incoherent scattering coefficient, with a longer correlation length leading to an increase in the incoherent scattering coefficient near the mirror angle and a decrease at other scattering angles. Additionally, for a fixed roughness and incident angle, with the increase in the ratio of the cylinder radius to the beam waist radius, the energy of the scattered light field is more concentrated. Our conclusion can provide a deeper understanding of the cylindrical scattering field, and also provide a basis for the study of rough cylindrical targets with different materials and scenes incident by Gaussian beam, and also provide a research basis for the scattering field

and speckle characteristics of complex composite rough targets that we will discuss in the future.

Author Contributions: Conceptualization, S.Y.; methodology, S.Y.; software, S.Y.; validation, S.Y.; writing—original draft preparation S.Y.; formal analysis, Z.W.; investigation, D.W.; writing—review and editing, Z.F. and C.C.; funding acquisition, G.F. All authors have read and agreed to the published version of the manuscript.

Institutional Review Board Statement: Not applicable.

Informed Consent Statement: Not applicable.

Data Availability Statement: Data are available on request due to restrictions, e.g., privacy or ethical.

Conflicts of Interest: The authors declare no conflict of interest.

References

1. Ogilvy, J.A. Wave scattering from rough surfaces. *Appl. Acoust.* **1995**, *45*, 93–94. [CrossRef]
2. Sun, B.Q.; George, W.K.; Yang, P.; Michael, S.T.; James, M.S. Simulation of the scattering properties of a chain-forming triangular prism oceanic diatom. *J. Quant. Spectrosc. Radiat. Transf.* **2016**, *178*, 390–399. [CrossRef]
3. Yadav, S.A.; Prasad, R.; Yadav, V.P.; Singh, S.K.; Sharma, J.; Srivastava, P.K. Far-field bistatic scattering simulation for rice crop biophysical parameters retrieval using modified radiative transfer model at X- and C-band. *Remote Sens. Environ.* **2022**, *272*, 112959. [CrossRef]
4. Ruiz-Cortés, V.A.; Dainty, J.C. Experimental light-scattering measurements from large-scale composite randomly rough surfaces. *J. Opt. Soc. Am. A Opt. Image Sci. Vis.* **2002**, *19*, 2043–2052. [CrossRef] [PubMed]
5. González-Aclalde, A.K.; Banon, J.P.; Oyvind, S.H.; Maradudin, A.A.; Simonsen, I. Experimental and numerical studies of the scattering of light from a two-dimensional randomly rough interface in the presence of total internal reflection: Optical Yoneda peaks. *Opt. Express* **2016**, *24*, 25995–26005. [CrossRef] [PubMed]
6. Andrey, V.O.; Sergei, A.T. Method of physical optics. In *Modern Electromagnetic Scattering Theory with Applications*; Wiley: Hoboken, NJ, USA, 2013; pp. 110–115.
7. Elfouhaily, T.M. A critical survey of approximate scattering wave theories from random rough surfaces. *Waves Random Media* **2004**, *14*, R1. [CrossRef]
8. Berlasso, R.G.; Quintián, F.P.; Rebollo, M.A.; Gaggioli, N.G.; Bernabeu, M.E. Speckle size of light scattered from slightly rough cylindrical surfaces. *Appl. Opt.* **2002**, *41*, 2020–2027. [CrossRef]
9. Zhang, G.; Wu, Z.S. Two-frequency mutual coherence function of scattering from arbitrarily shaped rough objects. *Opt. Express* **2011**, *19*, 7007–7019. [CrossRef]
10. Wu, Z.S.; Li, Y.Q. Scattering of a partially coherent Gaussian-Schell beam from a diffuse target in slant atmospheric turbulence. *J. Opt. Soc. Am. A Opt. Image Sci. Vis.* **2011**, *28*, 1531–1539. [CrossRef]
11. Collin, R.E. Scattering of an incident Gaussian beam by a perfectly conducting rough surface. *IEEE Trans. Antennas Propag.* **1994**, *42*, 70–74. [CrossRef]
12. Chen, H.; Wu, Z.S.; Yang, R.K.; Bai, L. Gaussian beam scattering from arbitrarily shaped objects with rough surfaces. *Waves Random Media* **2004**, *14*, 277–286. [CrossRef]
13. Gerald, M.; Wang, Q. Gaussian Beam Scattering from a Deterministic Rough Metal Surface. *IEEE Trans. Antennas Propag.* **2016**, *64*, 1868–1876.
14. Utsugi, T.; Goban, A.; Tokunaga, Y. Gaussian-wave-packet model for single-photon generation based on cavity quantum electrodynamics under adiabatic and nonadiabatic conditions. *Phys. Rev. A* **2022**, *106*, 023115. [CrossRef]
15. Odrigues Gonçalves, M.; Rozenman, G.G.; Zimmermann, M. Bright and dark diffractive focusing. *Appl. Phys. B* **2022**, *128*, 51. [CrossRef]
16. Rozenman, G.G.; Zimmermann, M.; Efremov, M.A. Projectile motion of surface gravity water wave packets: An analogy to quantum mechanics. *Eur. Phys. J. Spec. Top.* **2021**, *230*, 931–935. [CrossRef]
17. González, L.; Lindh, R. *Quantum Chemistry and Dynamics of Excited States: Methods and Applications*; John Wiley & Sons: New York, NY, USA, 2020; pp. 413–433.
18. Dijk, W.V.; Sprung, D.W.L.; Castonguay-Page, Y. Tunnelling of Hermite Gaussian wavepackets. *Phys. Scr.* **2020**, *95*, 065223–065238. [CrossRef]
19. Huang, Z.; Zhu, W.; Feng, Y.; Deng, D. Spatiotemporal self-accelerating Airy–Hermite–Gaussian and Airy–helical–Hermite–Gaussian wave packets in strongly nonlocal nonlinear media. *Opt. Commun.* **2019**, *441*, 195–207. [CrossRef]
20. Ishimaru, A. *Wave Propagation and Scattering in Random Media*; Academic Press: New York, NY, USA, 1978; pp. 400–410.

21. Bass, F.G.; Fuks, I.M. *Wave Scattering from Statistically Rough Surfaces*; Pergamon Press: New York, NY, USA, 1979; pp. 600–610.
22. Carterw, H. Electromagnetic field of a Gaussian beam with an rlliptical cross section. *J. Opt. Soc. Am.* **1972**, *62*, 1195–1201. [CrossRef]
23. Wuz, S.; Cao, S.M. Bistatic scattering by arbitrarily shaped objects with rough surface at optical and infrared frequencies. *Int. J. Infrared Millim. Waves* **1992**, *13*, 537–549.
24. Thorsos, E.I. The validity of the Kirchhoff approximation for rough surface scattering using a Gaussian roughness spectrum. *J. Acoust. Soc. Am.* **1988**, *83*, 78–92. [CrossRef]
25. Wait, J.R. The electromagnetic fields of a horizontal dipole in the presence of a conducting half-space. *Can. J. Phys.* **1961**, *39*, 1017–1028. [CrossRef]
26. Li, X.G.; Kim, C. Study on the two-frequency scattering cross section and pulse broadening of the one-dimensional fractal sea surface at millimeter wave frequency. *Prog. Electromagn. Res.* **2002**, *37*, 221–234.